Comparison of statistical model calculations for stable isotope neutron capture

M. Beard,[1,2,*] E. Uberseder,[1,†] R. Crowter,[1] and M. Wiescher[1]

[1]*Department of Physics, University of Notre Dame, Notre Dame, Indiana 46556, USA*

[2]*ExtreMe Matter Institute EMMI, GSI Helmholtzzentrum für Schwerionenforschung, Planckstraße 1, 64291 Darmstadt, Germany*

(Received 24 February 2014; revised manuscript received 28 July 2014; published 29 September 2014)

It is a well-observed result that different nuclear input models sensitively affect Hauser-Feshbach (HF) cross-section calculations. Less well-known, however, are the effects on calculations originating from nonmodel aspects, such as experimental data truncation and transmission function energy binning, as well as code-dependent aspects, such as the definition of level-density matching energy and the inclusion of shell correction terms in the level-density parameter. To investigate these aspects, Maxwellian-averaged neutron capture cross sections (MACS) at 30 keV have been calculated using the well-established statistical Hauser-Feshbach model codes TALYS and NON-SMOKER for approximately 340 nuclei. For the same nuclei, MACS predictions have also been obtained using two new HF codes, CIGAR and SAPPHIRE. Details of these two codes, which have been developed to contain an overlapping set of identically implemented nuclear physics input models, are presented. It is generally accepted that HF calculations are valid to within a factor of 3. It was found that this factor is dependent on both model and nonmodel details, such as the coarseness of the transmission function energy binning and data truncation, as well as variances in details regarding the implementation of level-density parameter, backshift, matching energy, and giant dipole strength function parameters.

DOI: 10.1103/PhysRevC.90.034619 PACS number(s): 24.60.Dr, 25.40.Lw, 25.70.Gh

I. INTRODUCTION

Information about nuclear reactions is of huge value for a myriad of applications. At present, transmutation via neutron reactions is one of the leading avenues of research in the disposal of long-lived isotopes, produced during nuclear-reactor fuel cycles. In this context, several new facilities at neutron sources have been developed, including the γ-calorimeter DANCE at the Los Alamos Neutron Science Center [1], n_TOF at CERN [2], GELINA at Institute for Reference Materials and Measurements [3], and the nELBE at Helmholtz-Zentrum Dresden-Rossendorf [4]. In addition, nuclear reactions are an essential input into the production of isotopes for both medical and fundamental research purposes. Within this framework, radiative neutron capture on stable nuclei can be used to produce short-lived products that can be purposed as tracers and γ-ray sources for targeted medical therapy and for industrial applications. Nuclear reaction rates are also the primary ingredient in nucleosynthesis studies. Neutron capture is of particular importance because it is by far the most dominant method for synthesizing nuclei heavier than iron. Indeed, virtually all of the heavy nuclei above iron in the solar system were produced via either the s(low) or r(apid) capture of neutrons [5].

Understanding nucleosynthesis processes requires the knowledge of a vast amount of cross-section information, the overwhelming majority of which is not experimentally known. In an attempt to bolster the dearth of experimental data, theoretical techniques must be employed to fill in the missing cross sections. Of crucial importance to the success of theoretical efforts, is the development of sound nuclear reaction models. The Hauser-Feshbach (HF) statistical model [6,7] is one such approach and has been widely used in nucleosynthesis studies. The central requirement for the reliable application of the statistical model is a high level density, usually estimated to be between five and ten resonances per MeV [8], so that resonance spacing overlaps and the reaction can be considered in terms of averaged quantities. There are some limitations to the HF approach, however. For instance, the level-density criteria may not be satisfied in light nuclei or for reactions involving nuclei near closed shells or close to driplines, where the lower Q values typically mean that compound nuclei are produced with low excitation energy. To obtain the cross section in these instances nonstatistical, single-resonance or direct capture models must be utilized [9]. Cross-section calculations from HF can, however, be complemented by including a component from direct capture to bound states. In principle, a full treatment of the direct capture component should include calculating the overlap of entrance channel wave function, the bound-state wave function, and the multipole transition operator. For s-wave neutron capture, however, it is possible to take advantage of the $1/\sqrt{E}$ dependence of the cross section to construct a simple model which can provide an estimate of the cross section at low energies in the compound nucleus. The HF picture is also invalid if the incident particle energy is sufficiently large so that the newly formed compound nucleus does not fully equilibrate before breaking apart. Reactions occurring before complete thermodynamic equilibrium are known as preequilibrium reactions, and must be treated by other methods [10,11]. For the majority of astrophysical applications however, preequilibrium contributions to the cross section can be neglected.

A statistical model calculation requires a number of nuclear physics inputs, including ground-state properties, such as masses and deformations, level-density descriptions, particle

*mbeard@nd.edu

†Current address: Cyclotron Institute, Texas A & M University, Collage Station, TX 77843, USA.

optical potential models, and γ-strength functions, which characterize the emission and absorption of photons. It is the various details of these numerous input parameters that really determine the success of a statistical model calculation. In principle, it would be possible to tailor each required input to yield the absolutely best HF description of a specific reaction. This approach can work well when limited to only a handful of individual reactions. However, there is a long tradition of using the HF model as a workhorse for generating large databases of cross sections and reaction rates for use in nucleosynthesis studies [12–15], and, provided that the criteria on level density and reaction energy are met, it is well suited for this application. The downside, however, is that when generating a library of reactions, it is simply not feasible to tune nuclear inputs from reaction to reaction. Instead global models that reliably describe the requisite nuclear models, preferably from stability to the driplines, are an outright necessity.

The HF model has become integral to numerous applications, including nuclear reactor and medical technologies and nucleosynthesis studies. As a result of the high demand for good-quality calculations, there is a long legacy of statistical model codes in the literature. Some of the most prominent codes used for nucleosynthesis applications today include SMOKER [14], NON-SMOKER [15,16], TALYS [17], EMPIRE [18], MOST [19], and SMARAGD [20,21]. In each case, a user performs a calculation by choosing between various models for the required nuclear inputs. Though each of these codes employs the same basic mathematical picture to calculate cross sections, it is often the case that different code packages present the user with a different selection of nuclear input models to choose from. Coupled with this, even where there is a common component, i.e., the backshifted Fermi gas model for predicting the level density, it is often the case that model-specific details, such as the backshift or level-density parameter, are at variance. An additional complication stems from the fact that, presumably because of historical computing considerations, not all codes use the same quantity of experimental data to perform a calculation. The combination of these factors make it exceedingly challenging to directly, and reliably, compare calculations from different HF code packages. However, because statistical model calculations are so intrinsic to nuclear applications, a comparative evaluation of the major aspects of some of the most commonly used HF codes is worthwhile.

The motivation of this paper is to compare (n,γ) HF cross section calculations from four code packages to highlight and evaluate uncertainties originating from model implementation details, as well as from nonmodel sources. This is done in the following sections through the context of radiative neutron capture reactions, predominantly on stable isotopes. It is stressed that the aim of this paper is not to produce an extensive set of neutron capture reactions for use in nucleosynthesis studies, but rather to provide an evaluation of cross-section uncertainties arising from model implementation and nonmodel sources. To this aim the code packages considered in the present study are: (1) TALYS (version 1.6); (2) NON-SMOKER; (3) CIGAR (Capture Induced Gamma-ray Reactions); (4) SAPPHIRE (Statistical Analysis for Particle and Photon Capture and Decay of High Energy Resonances) [22]. Of these, code packages TALYS and NON-SMOKER have been used to generate theoretical contributions for some of the most influential thermonuclear reaction rate libraries in nuclear astrophysics, BRUSLIB [23] and REACLIB [24]. CIGAR is based on the well-known SMOKER code [14] and includes an updated treatment of both the level density and the $E1$, $M1$, and $E2$ γ-strength functions, as well as the implementation of the latest experimental mass and nuclear excitation level data. SAPPHIRE is an independent code which can calculate both radiative capture and inverse cross sections. Both CIGAR and SAPPHIRE are new codes that have been developed to contain an identical set of nuclear input models, the intention being to investigate the impact on calculations arising from nonmodel aspects, such as the use of a truncated experimental data set.

It is informative to evaluate the various HF codes examined in this study by comparing the calculated cross sections to a "standard" result. It is advantageous to require an experimental value as the standard, because this removes any code-dependent complications that could occur from using a theoretical value. In practice, the requirement restricts the present study to nuclei on, or close to, the valley of stability for which data exist. However, this limitation is not a handicap to the present aim. Because the present work focuses on radiative neutron capture, it is natural to use the experimental neutron capture data contained in the KADoNiS database [25] as the standard. KADoNiS is a library of Maxwellian-averaged cross sections, compiled for approximately 350 isotopes, on and close to the valley of stability, for temperatures ranging from $T = 0.058$ GK to $T = 1.16$ GK. Because it is well known that HF calculations are not valid for light nuclei, the present study has focused on nuclei with neutron number $N \geqslant 20$, comparing the reaction rate to the KADoNiS Maxwellian-averaged cross sections at 30 keV.

The paper is organized as follows. In Sec. II the general method for calculating HF cross sections is described, and the major ingredients for a statistical model calculation are summarized. Maxwellian-averaged cross sections are also discussed. Details of the CIGAR and SAPPHIRE codes are presented in Sec. III. A comparative discussion of the results from TALYS, NON-SMOKER, CIGAR, and SAPPHIRE are presented in Sec. IV. Finally, conclusions are summarized in Sec. V.

II. STATISTICAL MODEL

The HF model is centered on the formation of a compound nucleus, which decays into energetically open channels after all of the reaction energy been fully shared out among the compound nucleons. It is generally accepted that over an energy range of 10 keV–10 MeV, the HF model is valid to within a factor of about 3 [12,15]. For energies less than this, not enough levels contribute to the cross section to allow the calculation of averaged transmission coefficients and so the validity of the statistical model breaks down. However, at neutron energies higher than 10 MeV, preequilibrium reactions, which occur before the compound nucleus has fully energy equilibrated, begin to contribute to the reaction cross section. Aside from the energy, angular momentum and parity, all of the information regarding the formation

of the compound is lost. The probability that a nuclear reaction will occur is governed by transmission coefficients: The transmission coefficient in the entrance channel for the formation of the compound nucleus and the transmission function for the corresponding decay into a given exit channel. The transmission coefficients themselves can be obtained by solving the Schrödinger equation with an optical nucleon-nucleus potential, in the case of particles, or a parametrization of the giant dipole resonance (GDR), in the case of photons (described in Sec. II B).

In the context of the statistical model, the cross section σ_{ij} for the reaction $i^\mu + j \rightarrow o + m^\nu$ is given by

$$\sigma(i^\mu(j,o)m^\nu,e_{ij}) = \frac{\pi}{k_{ij}^2(2J_i^\mu+1)(2J_j+1)} \times \sum_{J,\pi}(2J+1) \times \frac{T_j^\mu(E,J,\pi;E_i^\mu,J_i^\mu,\pi_i^\mu;E_j,J_j,\pi_j)T_o^\nu(E,J,\pi;E_m^\nu,J_m^\nu,\pi_m^\nu;E_o,J_o,\pi_o)}{T_{\rm tot}(E,J,\pi)}, \quad (1)$$

where target nucleus i is in the excited state μ and residual nucleus m is left in the excited state ν. The spin, parity, and excitation energy of the compound nucleus are given by J, π, and E, respectively. Spin, parity, and energy for a specific state in i (m) are represented by J_i^μ (J_m^ν), π_i^μ (π_m^ν), and E_i^μ (E_m^ν), respectively, whereas the spin, parity, and energy of j (o) are denoted by J_j (J_o), π_j (π_o), and E_j (E_o). k_{ij} is the wave number of the projectile and is equal to $k_{ij} = \sqrt{2\hat{A}_{ij}E_{\rm c.m.}}/\hbar$, where $\hat{A}_{ij}$ is the reduced mass and $E_{\rm c.m.}$ is the center-of-mass energy. The transmission functions for the formation and decay channels, as well as the total transmission function for the decay of the compound nucleus, are represented by T_j^μ, T_o^ν, and $T_{\rm tot}$, respectively.

For astrophysical applications, the total cross section $\sigma(i^\mu(j,o)m)$, i.e., summed over all possible residual excitation states ν, is frequently of more interest than cross sections to specific J_m^ν, π_m^ν, E_m^ν states. In this case, T_o replaces T_o^ν in Eq. (1), where

$$T_o(E,J,\pi;E_o,J_o,\pi_o) = \sum_\nu T_o(E,J,\pi;E_m^\nu,J_m^\nu,\pi_m^\nu;E_o,J_o,\pi_o), \quad (2)$$

and the sum ν is performed over all excited states in m. In practice, the sum over ν in Eq. (2) can involve a huge number of terms. Whenever excitation states at energies greater than $E_m^{\rm max}$, the maximum experimentally known energy, spin and parity become important; the sum must be replaced with an integral over the level density, $\rho(E_m,J_m,\pi_m)$:

$$T_o(E,J,\pi;E_o,J_o,\pi_o) = \sum_\nu^{E_m^\nu<E_m^{\rm max}} T_o^\nu(E,J,\pi;E_m^\nu,J_m^\nu,\pi_m^\nu;E_o,J_o,\pi_o) + \sum_{J_m,\pi_m}\int_{E_m^{\rm max}}^{E-E_m^0} T_o(E,J,\pi;E_m,J_m,\pi_m;E_o,J_o,\pi_o) \times \rho(E_m,J_m,\pi_m)dE_m. \quad (3)$$

In addition to considering a range of energetically possible states for the residual nucleus ν, in astrophysical environments thermal population of the target nucleus i, e.g., i^μ, must also be considered. In this case Eq. (1) must be modified to also include a sum over μ. In the laboratory, however, where target nuclei occupy their respective ground states, the sum over μ can be discounted. Consequently, it is the laboratory cross section, $\sigma_{ij}^{\rm lab} = \sum_\nu \sigma(i^{\mu=0} + j \rightarrow o + m^\nu)$, which is actually measured. It is understood that in the context of the present study the term "cross section" refers to $\sigma_{ij}^{\rm lab}$, and not the cross section which is obtained by considering the various thermally populated states of i.

For nuclear astrophysics studies, the reaction rate is a more useful quantity than the cross section because it accounts for the velocity distribution of the interacting particles in the stellar plasma. By folding the Maxwell-Boltzmann velocity distribution v of reactants i and j with $\sigma_{ij}^{\rm lab}$, the reaction rate can be expressed as $\langle\sigma_{ij}^{\rm lab}v\rangle$, the ground-state reaction rate per particle pair. For neutron capture reactions, however, which are the subject of the present work, it is customary to express $\langle\sigma_{ij}^{\rm lab}v\rangle$ in terms of the Maxwellian-averaged cross section (MACS), defined by

$$\langle\sigma_{ij}^{\rm lab}\rangle_T = \frac{\langle\sigma_{ij}^{\rm lab}v\rangle}{\sqrt{2k_BT/\hat{A}_{ij}}}, \quad (4)$$

where k_B is the Boltzmann constant and T the temperature. The quantity under the square root in Eq. (4) is actually the mean thermal velocity v_T at T. For a given temperature, the MACS differs from $\langle\sigma_{ij}^{\rm lab}v\rangle$ by a factor of thermal velocity. Typically, it is the ground-state MACS that is published in literature. There have been several attempts over the past decades to tabulate MACS values [26–29]. This has culminated in a collection of 356 recommended semiempirical and experimental MACS known collectively as the KADoNiS database [25].

A. Level density

Two descriptions of level density ρ are frequently used, often in combination and matched at some energy. The first is the well-known backshifted Fermi gas (BSFG) formula [30]. The "backshifted" part of the model considers the effect on the excitation energy E of breaking apart a pair of nucleons, a phenomena which must occur before individual nucleons can be excited in the nucleus. Assuming an equiparity of negative and positive parities, the BSFG level density is determined from

$$\rho(U,J,\pi) = \frac{\rho(U)_{\rm BSFG}S(U,J)}{2}, \quad (5)$$

where $U = E - \delta$ is an effective excitation energy, dependent on the backshift parameter δ. By including the backshift in the definition of U and according δ some mass dependence, it can be used to simulate the odd-even effects in nuclei. The spin dependence factor is denoted by $S(U,J)$, and is equal to

$$S(U,J) = \frac{2J+1}{2\sigma} e^{-J(J+1)/2\sigma^2} \tag{6}$$

and

$$\rho(U)_{\mathrm{BSFG}} = \frac{1}{12\sqrt{2}\sigma(aU^5)^{1/4}} e^{2\sqrt{aU}}, \tag{7}$$

in which a is a crucial aspect of the level density, known as the "level-density parameter," and σ is the spin cutoff parameter. For the BSFG model, the description of σ includes a dependence on atomic mass number and excitation energy. It was demonstrated in Ref. [31] that the current descriptions of σ agree well where discrete level data is available, but agreement between predictions strongly deteriorates with increasing excitation energy. One commonly used description is based on the assumption of the nucleus as a rigid rotating spherical body and is given by

$$\sigma^2 = 0.0145 A^{5/3} \sqrt{\frac{U}{a}}. \tag{8}$$

Equation (5) is essentially dependent on two quantities, a and δ. Both parameters can be obtained from fitting experimental resonance spacing data.

One drawback of the BSFG model, however, is that as $U \to 0, \rho \to \infty$. As a result, the BSFG model is unphysical for $E = \delta$. A second commonly used model, known as the constant temperature (CT) model [30], does not suffer from this limitation. The CT model is based on the observation that at low energy the number of excitation levels in the nucleus scales exponentially according to

$$N(E) = \exp\left[\frac{E - E_0}{T}\right], \tag{9}$$

where E_0 is a free parameter and T is the nuclear temperature. The level density is given by

$$\rho(U)_{\mathrm{CT}} = \frac{1}{T} e^{(E-E_0)/T}. \tag{10}$$

In practice, statistical model codes frequently use a composite of CT and BSFG models. In this approach the CT is used for excitation energies up to some matching point energy, while the BSFG model is used for higher energies.

Aside for the BSFG and CT level-density models, there are a large number of other frameworks for determining level density on the market. These include the generalized superfluid model (GSM) [32,33], which takes into account the effects of superconducting pairs, as well as microscopic and shell-model Monte Carlo approaches [34–37]. On and close to stability, good agreement has been found between predictions from BSFG and microscopic level-density models compared to D_o data [38]. However, for nuclei far from stability, it has been shown that strong differences between BSFG and microscopic level-density predictions can occur [39].

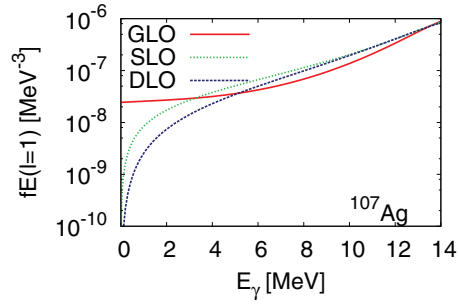

FIG. 1. (Color online) $E1$ ^{107}Ag strength function for three commonly used models, GLO [42], SLO [40,41], and DLO [43]. For the depicted GLO curve the initial excitation energy was 7.27 MeV.

B. Photon-transmission coefficient

The total photon-transmission coefficient is primarily composed of the sum of electric ($E1$) and magnetic ($M1$) dipole terms. Typically, T_{E1} is described phenomenologically in terms of the γ-strength function (gSF), where the gSF is a parametrized Lorentzian representation of the GDR. There are a few phenomenological descriptions of the GDR that are commonly used for practical purposes. These include the Brink-Axel single Lorentzian [40,41] (SLO), the Kopecky-Uhl generalized, energy-damped Lorentzian [42] (GLO), and the energy-damped double Lorentzian [43] (DLO). Strength functions for these three models are shown in Fig. 1 for the nucleus ^{107}Ag. All three approaches require parametrized information about the GDR, most frequently the energy E_{GDR}, cross section σ_{GDR}, and width Γ_{GDR} of the GDR.

Aside from the GDR parameters, the GLO representation also requires the nuclear temperature of the final state reached after the emission, or absorption, of a photon. In the GLO formalism T_{E1} is expressed as a function of γ-ray energy according to

$$T_{E1}(E_\gamma) = 2\pi E_\gamma \frac{\sigma_{\mathrm{GDR}}\Gamma_{\mathrm{GDR}}}{3\pi^2\hbar^2c^2}\left[\frac{E_\gamma\Gamma(E_\gamma)}{\left(E_\gamma^2 - E_{\mathrm{GDR}}^2\right)^2 + E_\gamma^2\Gamma(E_\gamma)^2} + \frac{0.7\Gamma_{\mathrm{GDR}}4\pi^2T^2}{E_{\mathrm{GDR}}^5}\right]. \tag{11}$$

The inclusion of a temperature-dependent term prevents the γ-strength function from approaching zero in the limit of zero energy, but finite temperature. One disadvantage of using a Lorentzian to represent the γ-strength function is that the parametrization overestimates the strength below the neutron threshold. To account for the overestimate, the tail of the Lorentzian is usually damped at low energy [44]. For the GLO model this is achieved through the use of an energy-dependent width,

$$\Gamma(E_\gamma) = \Gamma_{\mathrm{GDR}} \frac{E_\gamma^2 + 4\pi^2T^2}{E_{\mathrm{GDR}}^2}. \tag{12}$$

In the DLO formalism, $T_{E1}(E_\gamma)$ is obtained from

$$T_{E1}(E_\gamma) = 2\pi \frac{\sigma_{\rm GDR}\Gamma_{\rm GDR}}{3\pi^2\hbar^2c^2}\frac{1+\chi}{3} \times \frac{E_\gamma^4\Gamma(E_\gamma)}{\left(E_\gamma^2 - E_{\rm GDR}^2\right)^2 + E_\gamma^2\Gamma(E_\gamma)^2}, \quad (13)$$

where $\chi = 0.2$ is the neutron-proton exchange term. Energy damping in the DLO model is facilitated by the term

$$\Gamma(E_\gamma) = \sqrt{\frac{E_\gamma}{E_{\rm GDR}}}. \quad (14)$$

GDR parameters required for Eqs. (11) and (13) can be obtained from experimental or theoretical databases, e.g., RIPL-3 [45]. If no data exist, estimates can be obtained from models or systematic relations.

Though computationally less expensive, the use of phenomenological descriptions for T_{E1} does have limitations. Specifically, deviations from the smooth Lorentzian curve arising, for instance, from pygmy dipoles, cannot be predicted from this approach. It has been argued that, for neutron-rich nuclei, strong pygmy resonances located below the neutron threshold could have an effect the neutron capture rate [46]. For a review on pygmy resonances, see Ref. [47], and references therein. Improved predictive power of microscopic gSF models far from stability may have the answer to this problem for reactions on exotic nuclei. However, for the reactions on or close to the valley of stability considered here, the shortcomings of phenomenological T_{E1} must be balanced against the major simplifying advantage of using an analytic global relation that can be easily applied to generating large sets of calculations.

Usually the $E1$ contribution is considered to be the most dominant term; however, this assumption may break down for nuclei located in regions of the chart of the nuclides for which magnetic rotation has also been observed [48]. Experiments have shown that these nuclei, which tend to be located in the vicinity of closed shells, exhibit enhanced dipole strength for γ-ray energies less than 3 MeV [49–52]. Recent shell-model calculations for the isotopes $^{94-96}$Mo indicate that the additional dipole strength is $M1$ in nature [53]. As yet, however, a physical mechanism for understanding the origin of the additional $M1$ strength has not been fully established. Consequently, the implementation of a more reliable $M1$ strength model into HF codes has yet to be realized. In the absence of a more complete model, for practical applications T_{M1} is normally described in terms of systematics. This can be done by either (1) normalizing T_{M1} to T_{E1} as a function of atomic mass number, or (2) assuming a simple $T_{M1} \propto E_\gamma^3$ dependence. Higher terms, e.g., $E2$, maybe included in the total photon-transmission coefficient calculation as well; however, they contribute a trivial amount to the total γ-strength function.

C. Neutron transmission coefficients

Particle-transmission functions are normally obtained from solving the Schrödinger equation with an optical model potential (OMP) for the nucleon-nucleus interaction. Historically, the nuclear potential has been described by the Woods-Saxon shape; however, a Woods-Saxon equivalent square well (ESqW) has long been used in cross-section calculations as a convenient way of parametrizing the transmission function [12,13,54–57].

As a response to the need for an improved approach to OMP, especially for nuclei far from stability [38], a semimicroscopic optical model was proposed by [58]. Known as the JLM semimicroscopic optical model, it is based on the Brueckner theory of infinite nuclear matter and Reid's hard core nucleon-nucleon interaction, folded with the radial nuclear-matter density of the target. The nuclear-matter density itself can be obtained from various calculations, provided, for instance, in Refs. [59–61]. For radiative capture reactions, however, the cross sections are not very sensitive to the choice of matter density model.

III. THE CIGAR AND SAPPHIRE STATISTICAL MODEL CODES

Aside from the HF nuclear input models discussed in the previous section, HF code packages contain model implementation details and nonmodel aspects, both of which can potentially affect the calculations. To investigate the latter, two statistical model codes have recently been developed at the University of Notre Dame. SAPPHIRE is a new code, written in C++, designed primarily to simulate the decay of excited nuclei via the Monte Carlo technique. SAPPHIRE generates realistic particle and γ-ray distributions resulting from the statistical decay of a compound nucleus having a predefined excitation energy, with decay probabilities based on the most recent experimental data compilations and state-of-the-art theoretical models. The code is designed for large-scale multiprocessing and therefore is ideal for the generation of the large theoretical data sets often needed to determine experimental response functions without the need of excessive approximations. The transmission functions needed to form the probability distribution functions for Monte Carlo are identical to those required to calculate HF cross sections; therefore, the code can be used to calculate astrophysical reaction rates.

CIGAR is a new generation of the well-known SMOKER [14] code and is written in FORTRAN. CIGAR is tailored specifically for the large-scale calculation of astrophysical reaction rates using the statistical model. Both CIGAR and SAPPHIRE consider a range of projectile nuclei, and include four exit channels, namely: (particle,n), (particle,p), (particle,α), and (particle,γ). SAPPHIRE has the additional ability to calculate cross sections for photon induced reactions. CIGAR and SAPPHIRE, when used for cross-section calculations, do not include preequilibrium reactions, which makes them well suited to astrophysical studies because in these environments incident particles have energies that are typically less than approximately 10 MeV.

Detailed information concerning the numerous requisite nuclear physics input models used by CIGAR and SAPPHIRE are available in full elsewhere in the literature. However, salient aspects regarding the various nuclear model input options are briefly recapped in the following subsections.

A. Masses

For the nuclei considered here, masses are from the Ame2012 atomic mass evaluation [62]. For calculations involving nuclei further from the valley of stability, if a required mass is not in the experimental compilation then it is determined via the finite-range droplet model (FRDM) [63] mass model. Data for the spins and parities of the relevant nuclei are supplied by the RIPL-3 database [45]. Whereas SAPPHIRE utilizes all experimentally known complete level data before invoking a level-density model, CIGAR truncates the available data to a maximum of 20 levels before considering the level scheme complete.

B. Level density

The level-density model included in the CIGAR and SAPPHIRE code packages is based on the BSFG model, matched to the CT formalism at some matching point energy. The CT is found from the relation

$$T = \frac{\sqrt{a E_m}}{\tilde{a}(1 + \delta W e^{-\gamma E_m})} - \frac{2E_m}{3}, \tag{15}$$

where $\tilde{a}$ is defined below, and the matching energy can be solved from the systematic relation

$$E_m = 2.5 + 150/A. \tag{16}$$

The level-density model implemented in CIGAR and SAPPHIRE is common to the NON-SMOKER statistical model code. In this model, an excitation-energy-dependent form of a [32,64] is adopted. The definition of a is given in Eq. (17). Following the arguments set out in Ref. [8], Eq. (17) has been implemented in CIGAR and SAPPHIRE using δW, which is the microscopic energy correction obtained from FRDM [63]. The parameters α, β, and γ can be constrained by fitting calculated a to experimental level-density data for a range of nuclei. This task was performed in Ref. [8]. The backshift is defined as the average of the neutron and proton pairing gaps, which are represented in Eq. (17) by Δ_{neut} and Δ_{prot}, respectively. The pairing gaps are obtained from the various binding energies, BE. The expressions for a and δ are

$$\begin{aligned}
a &= \tilde{a}\left(1 + \delta W \frac{1 - e^{-\gamma U}}{U}\right),\\
\tilde{a} &= \alpha A + \beta A^{2/3},\\
\delta &= \frac{1}{2}[\Delta_{\text{neut}}(Z,N) + \Delta_{\text{prot}}(Z,N)],\\
\Delta_{\text{neut}}(Z,N) &= \frac{1}{2}[2BE(Z,N) - BE(Z,N-1)\\
&\quad - BE(Z,N+1)],\\
\Delta_{\text{prot}}(Z,N) &= \frac{1}{2}[2BE(Z,N)\\
&\quad - BE(Z-1,N) - BE(Z+1,N)].
\end{aligned} \tag{17}$$

C. Photon-transmission coefficient

There are two shared possibilities for γ-strength function model which can be invoked in CIGAR and SAPPHIRE. The first of these is the DLO model, detailed in Ref. [43] and outlined in Eq. (13). The GDR input parameters are obtained from the methods detailed in Ref. [43]. The second model is the GLO representation, described in Ref. [42] and summarized by Eq. (11). When the GLO model is selected, GDR parameters are taken from the RIPL-3 [45] database. If no data are available (as is the case, for instance, for $Z < 14$), required parameters are calculated as they would be for the DLO model. For deformed nuclei, the formalism to obtain T_{E1} [either Eq. (13) or Eq. (11)] is invoked for both sets of GDR parameters. The total transmission function is then given by the sum of the two vibrational components, where the sum is performed by according the higher energy contribution twice the weight of the other.

The main difference between the two photon-transmission models is the prediction of the strength close to S_n, as well as how steeply the strength is predicted to drop off below the threshold. In general, the DLO model tends to predict more strength than the GLO model around S_n, but also predicts a more rapid decline in strength as $E_\gamma \to 0$ (see Fig. 1).

D. Neutron transmission coefficient

Finally, the semimicroscopic JLM model is included in CIGAR and SAPPHIRE for the particle optical model (see Sec. II C). The JLM potential needs to make use of a radial nuclear-matter density model. In the CIGAR and SAPPHIRE calculations, the matter density is obtained from Ref. [60].

IV. RESULTS AND DISCUSSION

To optimize the accessibility of the present section, it has been split into two subsections. The first examines the impact on the MACS arising from nonmodel aspects such as energy binning and level data truncation. The CIGAR and SAPPHIRE codes have been used to perform this investigation. The second section examines the impact on the calculations arising from model implementation details, such as level-density parameter, backshift, and GDR parameters and uses the CIGAR and TALYS codes and results from the NON-SMOKER code.

A. Nonmodel aspects

To investigate numerical effects arising from nonmodel aspects, the CIGAR and SAPPHIRE codes were used to calculate MACS at $kT = 30$ keV for ≈345 isotopes in the KADoNiS library [25]. Both sets of calculations were performed using the identically implemented nuclear input models: BSFG + CT level density, the JLM OMP, and the GLO γ-strength function. Only the ground-state cross sections (i.e., σ_{ij}^{lab}) were used in the calculation of the MACS. Shown in Fig. 2 in red and blue, respectively, are the SAPPHIRE and CIGAR MACS as a percentage difference to the KADoNiS values ($\langle\sigma v\rangle_{\text{calc}} - \langle\sigma v\rangle_{\text{exp}}/\langle\sigma v\rangle_{\text{exp}}) \times 100$. Plotting the percentage difference to the experimental values, rather than the absolute ratio, displays the results on a clearer, linear scale. Overall, both SAPPHIRE and CIGAR reproduce the data well; calculations are typically within a factor of 3 of the experimental MACS, which is in line with currently accepted HF uncertainties. Results from both

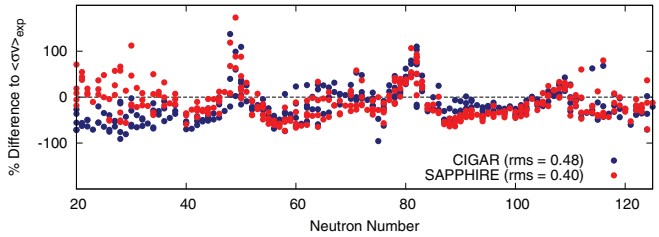

FIG. 2. (Color online) Red and blue points correspond to the percentage difference of $kT = 30$ keV MACS, calculated with SAPPHIRE and CIGAR, respectively, to the KADoNiS database. Calculations were performed using the γ-strength function from Ref. [42], the CT + BSFG level density with parameters from Ref. [8], and the optical model from Ref. [58].

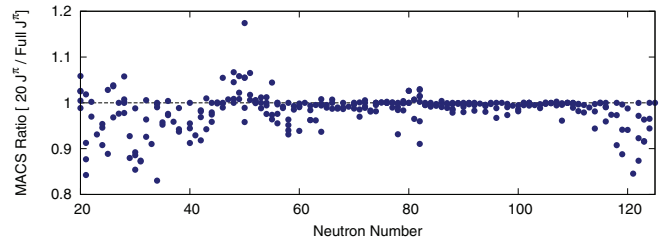

FIG. 3. (Color online) MACS calculated with SAPPHIRE obtained using truncated J^π data, compared to identical calculations performed using nontruncated J^π data. The level data are from RIPL-3 [45].

codes show that the largest deviations with the experimental values is around closed shells. Near closed shells, where Q values are low, the assumption of many closely spaced resonances in the compound nucleus is called into question. Consequently, the statistical model is not wholly applicable and performs poorly in those regions.

However, some minor differences in individual calculations can be observed between results from the two codes. Because the input models were the same, these variations can be attributed to computational differences between the codes. The differences are (i) the number of experimental levels J, with definite parity π, that are adopted for use in Eq. (2) before invoking a level-density model; and (ii) the coarseness of the transmission function energy grids. Statistical model Monte Carlo requires fine energy grids, whereas CIGAR has an energy binning optimized for the speed of calculation, which may not be ideal for all transmission function shapes. The impact of the coarser energy binning in CIGAR is particularly visible for nuclei with neutron numbers less than 40, where large differences between SAPPHIRE and CIGAR calculations are evident. In these cases, where it may not be wholly appropriate to use CIGAR with the GLO γ-strength function, SAPPHIRE may produce more accurate results owing to a better approximation of the integrated transmission function.

To estimate the uncertainty in calculations arising from using a truncated J^π scheme, two sets of identical calculations were performed using SAPPHIRE. In the first set of calculations, the truncation on J^π was dictated by the total amount of experimental data; i.e., all of the data in the RIPL-3 data base [45] was used. In the second set of calculations, the J^π data was truncated at 20 levels. The results from these two sets of calculations are compared in Fig. 3. The impact of the truncation is particularly evident for reactions involving low level densities, located around closed shells and $N < 40$. For these cases, where the statistical model is known to be less reliable, restricting the amount of J^π data used in calculations can affect the value of the theoretical MACS by almost 20%. That identical models, when used in different codes, can yield different results indicates that the current HF uncertainties are not strictly limited to the uncertainties associated with nuclear physics alone: Numerical effects inherent to a given code can also have an impact.

B. Model implementation

To investigate the impact on the calculation arising from model implementation details, identical calculations were performed with the code TALYS [17]. There are a large number of default nuclear input parameter settings in TALYS, all of which can be modified. To ensure that the comparison to Fig. 2 was as fair as possible, the same models were selected for the TALYS calculations, where available. With this in mind, the MACS were obtained using the CT + BSFG level-density formalism, as outlined in Sec. II A, as well as the GLO γ-strength function. By default, TALYS normalizes the γ-ray transmission coefficients to the average radiative capture width at the neutron threshold. This setting was initially disabled for the calculations presented here, so that the γ-strength function came directly from GDR parameters. Also by default, TALYS uses an experimentally derived level-density parameter a, if available. In the spirit of focusing the investigation on theoretical inputs only, this default was also initially disabled so that systematic formulas were used to obtain the requisite level-density input parameters (e.g., a, δ). Last, the particle-transmission functions were calculated using the semimicroscopic JLM optical potential, outlined in Sec. II C. In TALYS, the radial matter densities required by JLM are calculated with either the HFB-Skyrme or the HFB-Gogny interactions. TALYS uses only microscopic spherical contributions in the optical model calculation, but coupling to collective states, where such information exists, is also included by default in the total optical potential. For nuclei that have a coupling scheme, the inclusion of collective effects in the OMP increases the MACS by an amount which depends on the additional contribution to the transmission coefficient.

Plotted in solid blue circles in Fig. 4 are the TALYS MACS as a percentage difference to KADoNiS data. Comparing these points to those in Fig. 2 indicate that there are a number of differences between results from CIGAR (SAPPHIRE) and TALYS. Though all codes were operated using the CT + BSFG formalism, there are still deviations concerning precisely how the level density model has been applied; implementation of the matching energy between CT and BSFG, as well as the formalism for the spin cutoff parameter, the level-density parameter a and the backshift are not identical between the code packages. The sources and impact of the model implementation details are now discussed. For each difference investigated and presented below, the parameter of interest

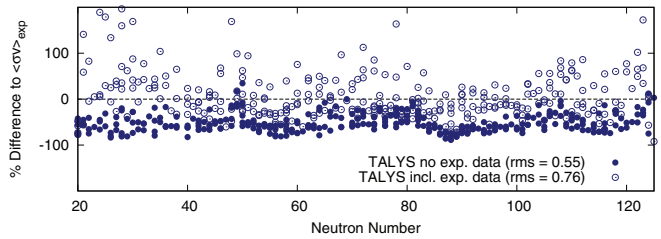

FIG. 4. (Color online) Percentage difference of $kT = 30$ keV MACS calculated with TALYS, compared to the KADoNiS database. For solid circles, calculations have been performed using the γ-strength function from Ref. [42], the CT + BSFG level density with parameters from Ref. [17], and the optical model from Ref. [58]. Open circles represent identical calculations; however, the TALYS default to use experimental level-density data has been adopted.

(i.e., matching energy, a, etc.) was first calculated for all of the nuclei using the TALYS code. The values of these parameters were then input directly in to the CIGAR code and used in new MACS calculations. The new CIGAR calculations were then compared to the original, "base" ones presented in Fig. 2. For optimum accessibility, listed below are each of the parameters investigated, along with a brief discussion of the respective impact. The convention adopted for Figs. 5, 6, 8, and 9 is as follows: Blue points refer to the ratio $\text{TALYS}_{\text{parameter}}/\text{CIGAR}_{\text{parameter}}$ and are plotted on the left axis, whereas red points indicate the ratio of $\text{MACS}_{\text{CIGAR+TALYSparameter}}/\text{MACS}_{\text{CIGAR}}$ and plotted on the right axis. For Fig. 7, the absolute value of the parameter is plotted on the left axis, the ratio of the MACS to the KADoNiS MACS are plotted on the right.

(1) *Temperature.* Shown in Fig. 5 is the ratio of the TALYS to CIGAR/SAPPHIRE CT. The TALYS CT is typically between ≈80% and 120% of the CIGAR/SAPPHIRE values, with larger deviations visible around closed shells. The ratio of the rates plotted on the right-hand axis shows that the rates are very insensitive to the CT: Even the largest temperature deviations result in no more than 5%–10% change in the MACS.

(2) *CT-BSFG matching point energy.* The ratio of the TALYS CT-BSFG matching energies to those used in CIGAR/SAPPHIRE are shown in Fig. 6. In general, TALYS does not obtain E_m systematically; instead, an iterative procedure is used to solve for matching energy [17]. Aside from a handful of examples, the matching point

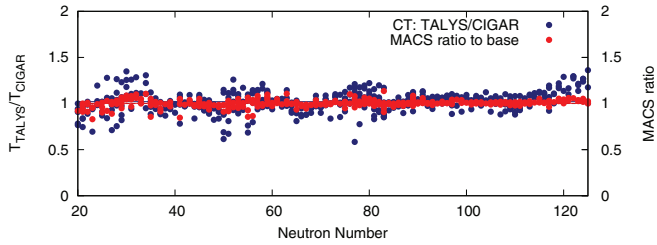

FIG. 5. (Color online) Left axis: Ratio of CT T calculated by TALYS to those calculated by CIGAR/SAPPHIRE using Eq. (15). Right axis: Ratio of CIGAR MACS using TALYS T to base CIGAR calculations.

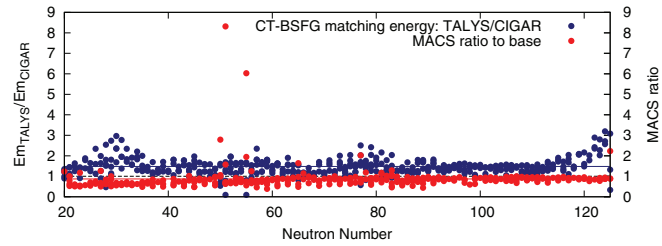

FIG. 6. (Color online) Left axis: Ratio of matching energies E_m calculated by TALYS to those calculated by CIGAR/SAPPHIRE using Eq. (16). Right axis: Ratio of CIGAR MACS using TALYS E_m to base CIGAR calculations.

energies used in TALYS are on average 50% larger than those obtained from Eq. (16). Compared to the CIGAR base MACS, calculations using TALYS E_m are, on average, 13% smaller.

(3) *Backshift.* For the CT option in TALYS, δ is found from the systematic formula

$$\delta = \chi \frac{12}{A^{1/2}}, \tag{18}$$

where $\chi = 0$, 1 or 2, for odd-odd, odd-even, or even-even isotopes, respectively. In CIGAR (SAPPHIRE), δ is determined from mass differences between neighboring nuclei [8]. As shown on the left axis in Fig. 7, the backshift obtained by these two different models varies from nucleus to nucleus, but can be a few MeV. The right axis of the figure shows the ratio of the MACSs obtained with each of the backshift models to the KADoNiS data: Open blue circles show the ratio of the cigar calculations using Eq. (17), open red circles show the ratio using cigar with Eq. (18) instead. Roughly, δ obtained from Eq. (18) result in MACSs that are 50% smaller than those calculated using Eq. (17).

(4) *Level-density parameter.* First, TALYS uses different values to CIGAR (SAPPHIRE) for the global parameters α, β, and γ required to find a from Eq. (17). Second, TALYS determines δW from differences between experimental and liquid drop masses, not the FRDM microscopic energy corrections used by CIGAR (SAPPHIRE). As shown on the left axis in Fig. 8,

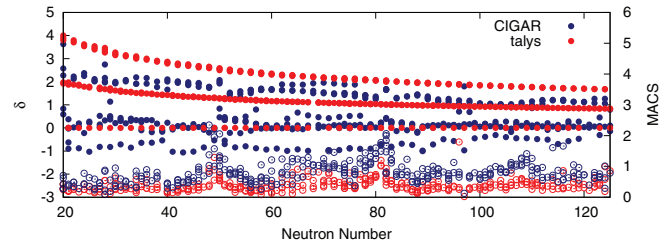

FIG. 7. (Color online) Left axis: Backshift as calculated in cigar(sapphire) using Eq. (17) (solid blue circles), and talys using Eq. (18) (solid red circles). Right axis: Ratio of CIGAR MACS to KADoNiS values. Open blue circles were obtained using Eq. (17); open red circles were obtained using Eq. (18).

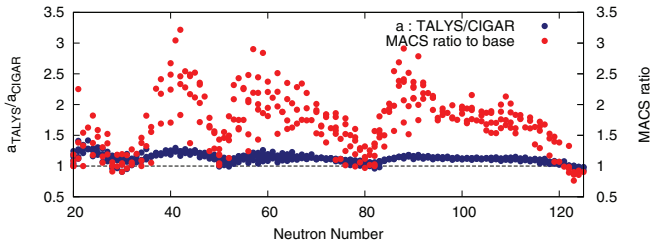

FIG. 8. (Color online) Left axis: Ratio of level-density parameter a at S_n calculated by TALYS to those calculated by CIGAR/SAPPHIRE using Eq. (17). Right axis: Red points show ratio of CIGAR MACS using TALYS a to base CIGAR calculations.

$a(S_n)_{\text{TALYS}} > a(S_n)_{\text{CIGAR(SAPPHIRE)}}$. The right axis of the figure shows how sensitive the MACS calculations are to a, particularly between shells, where rate enhancements of up to a factor of 3 are observed.

(5) *Spin cutoff parameter.* The default model for σ^2 in TALYS is given by

$$\sigma^2 = \frac{0.013\,89 A^{5/3}}{\tilde{a}} \sqrt{aU}, \tag{19}$$

whereas in CIGAR/SAPPHIRE it is given by Eq. (8). Around closed shells, the spin cutoff parameter from Eq. (19) is lower than that from Eq. (8), which, through Eq. (7), results in higher capture cross sections. The opposite is true between magic numbers. As shown in Fig. 9, the difference in the MACS from using either Eq. (19) or Eq. (8) can be up to 30%.

An additional source of difference between CIGAR (SAPPHIRE), on one hand, and TALYS, on the other, concerns the parameters that enter into the GDR calculation. TALYS uses a combination of experimental, where possible, and systematic data for GDR widths and energies. CIGAR and SAPPHIRE, however, use the theoretical compilation of Ref. [45]. Typically, the parameters used by CIGAR and SAPPHIRE are less than those used in TALYS calculations: E_{GDR} can be up to approximately 20% smaller, whereas Γ_{GDR} maybe within a factor of 2. Shown as open blue circles in Fig. 10 are the percentage difference to KADoNiS for MACSs calculated using the CIGAR code with the TALYS parameters. For comparison, the solid blue circles reproduce the original CIGAR calculations, shown in Fig. 2. In

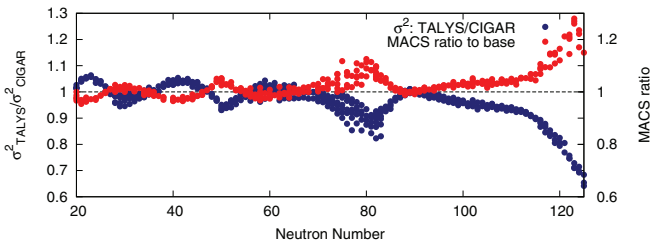

FIG. 9. (Color online) Left axis: Ratio of the spin cutoff parameter σ calculated by TALYS to those calculated by CIGAR/SAPPHIRE using Eq. (8). Right axis: Red points show ratio of CIGAR MACS using TALYS σ^2 to base CIGAR calculations.

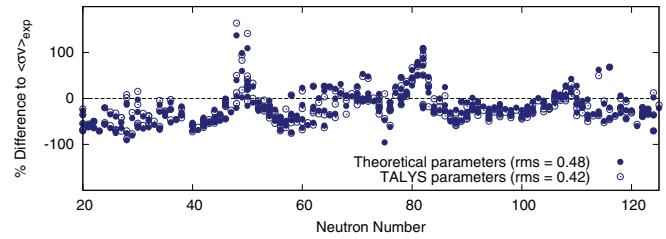

FIG. 10. (Color online) Percentage difference of $kT = 30$ keV MACS calculated with CIGAR, compared to the KADoNiS database. Solid blue circles have been calculated with GDR parameters from the theoretical compilation of Ref. [45]; open blue circles are identical calculations obtained using the experimental GDR parameters from Ref. [45].

general, the different GDR parameter sources result in only a few percent difference for any given nucleus.

As already mentioned, by default a great deal of experimental data can be used in a TALYS calculation. This includes experimental GDR parameters and the normalization of γ-ray transmission coefficients to average radiative capture widths, as well as experimental level-density data from s-wave capture neutron-resonance spacing and discrete levels data. Though disabled in the present study, for the majority of TALYS calculations appearing in the literature these defaults are usually adopted. For the sake of completeness, shown as open blue circles in Fig. 4 are TALYS MACSs at 30 keV as a percentage difference to KADoNiS values, obtained using the various experimental inputs. Because most often TALYS is used with default settings invoked, the γ-ray transmission coefficient normalization factor, which was disabled for the solid blue circles, was also enabled. This means that the γ-strength function was scaled to the average radiative capture width at the neutron threshold. The (n,γ) rate is extremely sensitive to the γ-ray transmission functions. Enabling this scaling parameter is the reason why the two sets of calculations look so different and why, for some nuclei, the agreement with KADoNiS MACS appears to be poorer with data included.

In addition to TALYS, CIGAR, and SAPPHIRE, calculations have also been compared to results from the NON-SMOKER code. Like CIGAR, NON-SMOKER also uses a J^π level scheme truncated to a maximum of 20 discreet levels. Depicted in Fig. 11 are NON-SMOKER MACS as a percentage difference to values in the KADoNiS database. Unfortunately, because the NON-SMOKER results are only available in tabulated form, it is not possible to perform calculations using a variety of models. However, because the NON-SMOKER database has

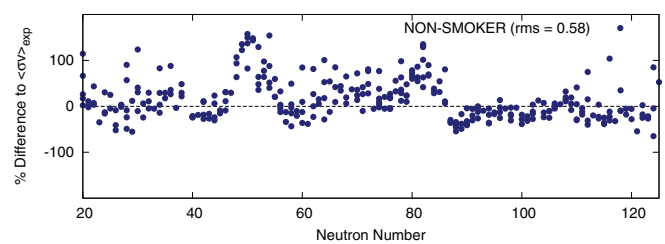

FIG. 11. (Color online) Percentage difference of $kT = 30$ keV MACSs calculated by NON-SMOKER. Rate data taken from Ref. [65].

been generated using the CT + BSFG level density with a and δ from Eq. (17), as well as the JLM optical model, the only major difference with CIGAR (SAPPHIRE) calculations is the γ-strength function. NON-SMOKER uses the DLO model, Eq. (13), where the required parameters are calculated via the methods set out in Ref. [43]. At low energies the γ-strength function is known to deviate from a Lorentzian representation. The additional energy damping is accounted for through the energy-dependent width, $\Gamma(E_\gamma)$, discussed in Sec. II B. As shown in Fig. 1, around the neutron threshold the DLO model overestimates the γ-strength function compared to the GLO representation. As a result, cross sections calculated using the DLO model tend to be larger.

The choice of γ-strength function has a significant impact on the MACS. Within the framework of HF theory, $\sigma(n,\gamma) \propto \frac{T_n T_\gamma}{T_{\text{tot}}}$, where T_{tot} represents the transmission to all possible energetically accessible channels. The transmission coefficients can be related to the average widths via $T = 2\pi\rho\langle\Gamma\rangle$, so that $\sigma(n,\gamma) \propto \frac{\langle\Gamma_n\rangle\langle\Gamma_\gamma\rangle}{\Gamma_{\text{tot}}}$. In general, $\langle\Gamma_n\rangle > \langle\Gamma_\gamma\rangle$ so that the neutron width dominates the photon width in the numerator. However, the neutron width is also the major constituent of the total transmission, so $\langle\Gamma_n\rangle$ cancels out with Γ_{tot} in the denominator, leaving $\sigma(n,\gamma) \propto \langle\Gamma_\gamma\rangle$. Consequently, for the (n,γ) reactions considered here, knowledge of the γ-strength function is more crucial than information on the neutron optical model, and cross sections tend to be less sensitive to choice of particle OMP [66]. For nuclei close to and on the valley of stability, enhancements and structure observed on the low-energy tail of the γ-strength function can wash out over the entire cross section [67]. However, for neutron-rich nuclei enhancement of the dipole strength below 3 MeV could have significant consequences [68].

V. CONCLUSIONS

It is widely accepted that HF calculations are uncertain to within a factor of three. That the selection of different nuclear models sensitively affects the HF calculations is well known. Presented here are the uncertainties from two sources, implementation details regarding specific models and nonmodel aspects. To investigate the latter uncertainties, two codes were developed, CIGAR, SAPPHIRE. The codes were designed to contain an identical set of nuclear inputs, e.g., level density, γ-ray strength function, and particle optical model, implemented with identical details, i.e., backshift, level-density parameter, GDR parameters, etc. By calculating MACSs for 340 isotopes in the KADoNiS database, variations between code calculations highlighted the uncertainties stemming from truncated data use and coarse transmission function energy binning. It was found that truncating the quantity of excitation level data in the SAPPHIRE calculation could result in as much as a 20% decrease in the calculated MACS. It was also observed that the speed-optimized, but coarse, energy binning can underestimate MACS, particularly for nuclei with low level densities.

To investigate the uncertainties associated with model implementation details, MACS calculations from CIGAR, TALYS, and NON-SMOKER were compared. Though in all cases MACSs were calculated using the same basic nuclear input models, there are still major differences regarding how backshift, level-density parameter, BSFG-CT matching energy, spin-cutoff parameter, and GDR parameters are obtained. Of the differences investigated in the present study, it was found, somewhat expectantly, that variations in the parameters entering into the BSFG level-density model were the most important. Of these, variations in level-density parameter were the most crucial, affecting the MACS calculations by up to a factor of three.

In the framework of calculating MACS at 30 keV, the present paper has attempted to highlight some of the crucial differences between the commonly used HF codes TALYS and NON-SMOKER. It is hoped that comparing input models and calculations from these two code packages will assist future users in interpreting their results.

ACKNOWLEDGMENTS

This work was supported by the Alliance Program of the Helmholtz Association (Grant No. HA216/EMMI) and by the Joint Institute for Nuclear Astrophysics (NSF Grant No. PHY08 22648). Discussions with T. Raucher, S. Goriely, and the talys team are gratefully acknowledged.

[1] R. Reifarth, E.-I. Esch, A. Alpizar-Vicente, E. Bond, T. Bredeweg, S. Glover, U. Greife, R. Hatarik, R. Haight, A. Kronenberg *et al.*, Nucl. Instrum. Methods Phys. Res., Sect. B **241**, 176 (2005).
[2] CERN n_TOF Facility Performance Report, 2002, http://www.cern.ch/n_tof.
[3] M. Flaska, A. Borella, D. Lathouwers, L. Mihailescu, W. Mondelaers, A. Plompen, H. van Dam, and T. van der Hagen, Nucl. Instrum. Methods Phys. Res., Sect. A **531**, 392 (2004).
[4] J. Klug, E. Altstadt, C. Beckert, R. Beyer, H. Freiesleben, V. Galindo, E. Grosse, A. Junghans, D. Lgrdy, B. Naumann *et al.*, Nucl. Instrum. Methods Phys. Res., Sect. A **577**, 641 (2007).
[5] F. Käppeler, R. Gallino, S. Bisterzo, and W. Aoki, Rev. Mod. Phys. **83**, 157 (2011).
[6] L. Wolfenstein, Phys. Rev. **82**, 690 (1951).
[7] W. Hauser and H. Feshbach, Phys. Rev. **87**, 366 (1952).
[8] T. Rauscher, F.-K. Thielemann, and K.-L. Kratz, Phys. Rev. C **56**, 1613 (1997).
[9] G. J. Mathews, A. Mengoni, F.-K. Thielemann, and W. A. Fowler, Astrophys. J. **270**, 740 (1983).
[10] E. Gadioli and P. E. Hodgson, *Pre-equilibrium Nuclear Reactions* (Oxford University Press, New York, 1982).
[11] A. Koning and M. Duijvestijn, Nucl. Phys. A **744**, 15 (2004).
[12] J. Holmes, S. Woosley, W. A. Fowler, and B. Zimmerman, At. Data Nucl. Data Tables **18**, 305 (1976).
[13] S. Woosley, W. A. Fowler, J. Holmes, and B. Zimmerman, At. Data Nucl. Data Tables **22**, 371 (1978).
[14] F.-K. Thielemann, M. Arnould, and J. W. Truran, in *Advances in Nuclear Astrophysics*, edited by E. Vangioni-Flam (Editions Frontiere, Gif sur Yvette, 1987), p. 525.

[15] T. Rauscher and F. K. Thielemann, At. Data Nucl. Data Tables **75**, 1 (2000).
[16] T. Rauscher and F.-K. Thielemann, in *Stellar Evolution, Stellar Explosions and Galactic Chemical Evolution*, edited by A. Mezzacappa (IOP, Bristol, 1998), p. 519.
[17] A. J. Koning, S. Hilaire, and M. Duijvestijn, in *ND 2007—International Conference on Nuclear Data for Science and Technology*, edited by O. Bersillon, F. Gunsing, E. Bauge, R. Jacqmin, and S. Leray (EDP Sciences, Les Ulis, France, 2008), p. 211.
[18] M. Herman, R. Capote, B. Carlson, P. Obloinsk, M. Sin, A. Trkov, H. Wienke, and V. Zerkin, Nucl. Data Sheets **108**, 2655 (2007).
[19] S. Goriely, in *Nuclei in the Cosmos V*, edited by N. Prantzos and S. Harissopulos (Editions Frontieres, Paris, 1999), p. 314.
[20] T. Rauscher, Int. J. Mod. Phys. E **20**, 1071 (2011).
[21] T. Rauscher, code SMARAGD, http://nucastro.org/smaragd.html.
[22] E. Uberseder, T. Adachi, T. Aumann, S. Beceiro-Novo, K. Boretzky, C. Caesar, I. Dillmann, O. Ershova, A. Estrade, F. Farinon *et al.*, Phys. Rev. Lett. **112**, 211101 (2014).
[23] Brussels library, http://www.astro.ulb.ac.be/bruslib.
[24] R. H. Cyburt, A. M. Amthor, R. Ferguson, Z. Meisel, K. Smith, S. Warren, A. Heger, R. D. Hoffman, T. Rauscher, A. Sakharuk *et al.*, Astrophys. J. Suppl. **189**, 240 (2010).
[25] I. Dillmann, R. Plag, F. Käppeler, and T. Rauscher, in *EFNUDAT Fast Neutrons: Scientific Workshop on Neutron Measurements, Theory and Applications* (JRC-IRMM, Geel, 2009).
[26] B. Allen, J. Gibbons, and R. Macklin, in *Advances in Nuclear Physics*, edited by M. Baranger and E. Vogt (Springer, New York, 1971), pp. 205–259.
[27] Z. Bao and F. Käppeler, At. Data Nucl. Data Tables **36**, 411 (1987).
[28] H. Beer, F. Voss, and R. R. Winters, Astrophys. J. Suppl. **80**, 403 (1992).
[29] Z. Bao, H. Beer, F. Käppeler, F. Voss, K. Wisshak, and T. Rauscher, At. Data Nucl. Data Tables **76**, 70 (2000).
[30] A. Gilbert and A. G. W. Cameron, Can. J. Phys. **43**, 1446 (1965).
[31] T. von Egidy and D. Bucurescu, Phys. Rev. C **80**, 054310 (2009).
[32] A. Ignatyuk, K. Istekov, and G. Smirenkin, Sov. J. Nucl. Phys. **29**, 450 (1979).
[33] A. V. Ignatyuk, J. L. Weil, S. Raman, and S. Kahane, Phys. Rev. C **47**, 1504 (1993).
[34] S. Goriely, S. Hilaire, and A. J. Koning, Phys. Rev. C **78**, 064307 (2008).
[35] S. Hilaire and S. Goriely, Nucl. Phys. A **779**, 63 (2006).
[36] Y. Alhassid, L. Fang, and H. Nakada, Phys. Rev. Lett. **101**, 082501 (2008).
[37] H. Uhrenholt, S. Åberg, A. Dobrowolski, T. Døssing, T. Ichikawa, and P. Möller, Nucl. Phys. A **913**, 127 (2013).
[38] M. Arnould and S. Goriely, Nucl. Phys. A **777**, 157 (2006).
[39] M. Arnould, S. Goriely, and K. Takahashi, Phys. Rep. **450**, 97 (2007).
[40] D. Brink, Nucl. Phys. **4**, 215 (1957).
[41] P. Axel, Phys. Rev. **126**, 671 (1962).
[42] J. Kopecky and M. Uhl, Phys. Rev. C **41**, 1941 (1990).
[43] F.-K. Thielemann and M. Arnould, in *Proceedings of the International Conference on Nuclear Data for Science and Technology*, edited by K. Böchoff (Reidel, Dordrecht, 1983), p. 762.
[44] C. M. McCullagh, M. L. Stelts, and R. E. Chrien, Phys. Rev. C **23**, 1394 (1981).
[45] R. Capote, M. Herman, P. Obloinsk, P. Young, S. Goriely, T. Belgya, A. Ignatyuk, A. Koning, S. Hilaire, V. Plujko *et al.*, Nucl. Data Sheets **110**, 3107 (2009).
[46] S. Goriely, Phys. Lett. B **436**, 10 (1998).
[47] D. Savran, T. Aumann, and A. Zilges, Prog. Part. Nucl. Phys. **70**, 210 (2013).
[48] S. Frauendorf, Rev. Mod. Phys. **73**, 463 (2001).
[49] M. Guttormsen, R. Chankova, U. Agvaanluvsan, E. Algin, L. A. Bernstein, F. Ingebretsen, T. Lönnroth, S. Messelt, G. E. Mitchell, J. Rekstad *et al.*, Phys. Rev. C **71**, 044307 (2005).
[50] M. Wiedeking, L. A. Bernstein, M. Krtička, D. L. Bleuel, J. M. Allmond, M. S. Basunia, J. T. Burke, P. Fallon, R. B. Firestone, B. L. Goldblum *et al.*, Phys. Rev. Lett. **108**, 162503 (2012).
[51] A. Voinov, E. Algin, U. Agvaanluvsan, T. Belgya, R. Chankova, M. Guttormsen, G. E. Mitchell, J. Rekstad, A. Schiller, and S. Siem, Phys. Rev. Lett. **93**, 142504 (2004).
[52] A. Voinov, S. M. Grimes, C. R. Brune, M. Guttormsen, A. C. Larsen, T. N. Massey, A. Schiller, and S. Siem, Phys. Rev. C **81**, 024319 (2010).
[53] R. Schwengner, S. Frauendorf, and A. C. Larsen, Phys. Rev. Lett. **111**, 232504 (2013).
[54] G. Michaud, L. Scherk, and E. Vogt, Phys. Rev. C **1**, 864 (1970).
[55] G. Michaud and W. A. Fowler, Phys. Rev. C **2**, 2041 (1970).
[56] G. J. Michaud and E. W. Vogt, Phys. Rev. C **5**, 350 (1972).
[57] Z. Fülöp, G. Gyürky, Z. Máté, E. Somorjai, L. Zolnai, D. Galaviz, M. Babilon, P. Mohr, A. Zilges, T. Rauscher *et al.*, Phys. Rev. C **64**, 065805 (2001).
[58] J.-P. Jeukenne, A. Lejeune, and C. Mahaux, Phys. Rev. C **16**, 80 (1977).
[59] M. Samyn, S. Goriely, P.-H. Heenen, J. Pearson, and F. Tondeur, Nucl. Phys. A **700**, 142 (2002).
[60] J. W. Negele, Phys. Rev. C **1**, 1260 (1970).
[61] S. Goriely, M. Samyn, and J. M. Pearson, Phys. Rev. C **75**, 064312 (2007).
[62] G. Audi, M. Wang, A. Wapstra, F. Kondev, M. MacCormick, X. Xu, and B. Pfeiffer, Chin. Phys. C **36**, 1287 (2012).
[63] P. Möller, J. R. Nix, W. D. Myers, and W. J. Swiatecki, At. Data Nucl. Data Tables **59**, 185 (1995).
[64] A. Ignatyuk, G. Smirenkin, and A. Tishin, Yad. Fiz. **21**, 485 (1975).
[65] T. Raucher, *Non-smoker database*, http://nucastro.org/websmoker.html.
[66] T. Rauscher, Astrophys. J. Suppl. Ser. **201**, 26 (2012).
[67] M. Beard, S. Frauendorf, B. Kämpfer, R. Schwengner, and M. Wiescher, Phys. Rev. C **85**, 065808 (2012).
[68] A. C. Larsen and S. Goriely, Phys. Rev. C **82**, 014318 (2010).